

Publication Year	2015
Acceptance in OA	2020-03-04T16:11:04Z
Title	Low-redshift quasars in the SDSS Stripe 82. Host galaxy colours and close environment
Authors	BETTONI, Daniela, Falomo, R., Kotilainen, J. K., Karhunen, K., USLENGHI, MICHELA
Publisher's version (DOI)	10.1093/mnras/stv2233
Handle	http://hdl.handle.net/20.500.12386/23122
Journal	MONTHLY NOTICES OF THE ROYAL ASTRONOMICAL SOCIETY
Volume	454

Monthly Notices
of the
ROYAL ASTRONOMICAL SOCIETY

MNRAS **454,** 4103–4113 (2015) doi:10.1093/mnras/stv2233

Low-redshift quasars in the SDSS Stripe 82. Host galaxy colours and close environment

D. Bettoni,[1⋆] R. Falomo,[1] J. K. Kotilainen,[2] K. Karhunen[3] and M. Uslenghi[4]

[1] *INAF – Osservatorio Astronomico di Padova, Vicolo dell'Osservatorio 5, I-35122 Padova (PD), Italy*
[2] *Finnish Centre for Astronomy with ESO (FINCA), University of Turku, Väisäläntie 20, FI-21500 Piikkiö, Finland*
[3] *Tuorla Observatory, Department of Physics and Astronomy, University of Turku, FI-21500 Piikkio, Finland.*
[4] *INAF-IASF via E. Bassini 15, I-20133 Milano, Italy*

Accepted 2015 September 23. Received 2015 September 23; in original form 2015 May 8

ABSTRACT

We present a photometrical and morphological multicolour study of the properties of low-redshift ($z < 0.3$) quasar hosts based on a large and homogeneous data set of quasars derived from the Sloan Digital Sky Survey (DR7). We used quasars that were imaged in the SDSS Stripe82 that is up to 2 mag deeper than standard Sloan images. This sample is part of a larger data set of ∼400 quasars at $z < 0.5$ for which both the host galaxies and their galaxy environments were studied. For 52 quasars, we undertake a study of the colour of the host galaxies and of their close environments in the u, g, r, i and z bands. We are able to resolve almost all the quasars in the sample in the filters g, r, i and z and also in u for about 50 per cent of the targets. We found that the mean colours of the QSO host galaxy ($g - i = 0.82 \pm 0.26$; $r - i = 0.26 \pm 0.16$ and $u - g = 1.32 \pm 0.25$) are very similar to the values of a sample of inactive galaxies matched in terms of redshift and galaxy luminosity with the quasar sample. There is a suggestion that the most massive QSO hosts have bluer colours. Both quasar hosts and the comparison sample of inactive galaxies have candidates of close (<50 kpc) companion galaxies for ∼30 per cent of the sources with no significant difference between active and inactive galaxies. We do not find significant correlation between the central black hole (BH) mass and the quasar host luminosity that appears to be extra luminous at a given BH mass with respect to the local relation ($M_{\rm BH} - M_{\rm host}$) for inactive galaxies. This confirms previous suggestion that a substantial disc component, not correlated with the BH mass, is present in the galaxies hosting low-z quasars. These results support a scenario where the activation of the nucleus has negligible effects on the global structural and photometrical properties of the hosting galaxies.

Key words: galaxies: active – galaxies: evolution – galaxies: nuclei – quasars: general.

1 INTRODUCTION

The characterization of the properties of the host galaxies of QSO is an important tool to investigate the role of the AGN in their evolution. In the last years, there is growing evidence that (see e.g. Schawinski et al. 2011; Heckman & Best 2014) AGN hosts are very similar in morphology to inactive galaxies at the same redshift. For instance, Cisternas et al. (2011) found that the host galaxies have normal morphologies in ∼85 per cent of their sample of X-ray bright AGN.

The characterization of the properties of AGN hosts offers also the opportunity to investigate the link between the central black hole (BH) mass and its host galaxy at moderate to high redshift and to trace the possible coevolution at different cosmic epochs. The mass of the central BH can be derived under the assumption that the broad emitting regions are under the sphere of influence of the supermassive BH (SMBH) using the virial method from the analysis of the broad emission lines of the QSO and from empirical relation between the continuum luminosity and the size of the broad-line region (Dunlop et al. 2003; Gultekin et al. 2009). Because of the high luminosity of QSO and the prominent emission lines, these can be done for a large number of sources using various emission lines (e.g. Shen et al. 2011).

On the other hand, the characterization of the properties of their host galaxies is more challenging because one has to decompose the starlight of the host galaxy from that of the nuclear emission. Since the nucleus is more luminous than the host galaxy, this observation

⋆ E-mail: daniela.bettoni@oapd.inaf.it

© 2015 The Authors
Published by Oxford University Press on behalf of the Royal Astronomical Society

requires excellent seeing conditions for ground-based observations or images obtained with *Hubble Space Telescope* (*HST*). In spite of these difficulties for several QSO, it was possible to deblend the nuclear and starlight contribution of quasars (see e.g. McLeod & Rieke 1995; Kotilainen & Falomo 2004; Falomo et al. 2014) using ground-based data or using *HST* imaging for relatively low ($z < 1$) redshift objects (see e.g. Bahcall et al. 1997; Kukula et al. 2001; Ridgway et al. 2001; Dunlop et al. 2003; Pagani, Falomo & Treves 2003; Floyd et al. 2004; Jahnke et al. 2009). For a limited number of QSOs, the use of 8–10 m telescope under superb seeing conditions or with adaptive optics imaging has allowed the study of quasar host at high redshift (Kotilainen et al. 2007, 2009) and/or with adaptive optics (Falomo et al. 2008). These observations allowed to trace a first view of the cosmic coevolution of SMBH and their host galaxies (see e.g. Decarli et al. 2010, 2012; Sanghvi et al. 2014).

A less explored issue is to assess the stellar population of the galaxies hosting active SMBH as compared with that of inactive galaxies. The understanding of the link between stellar population and growth and activation of a massive BH can in fact offers important clues to the role of merging for fuelling the central BH. Although galaxy interactions and merging have been long assumed as the main drive of the AGN phenomenon (e.g. Cisternas et al. 2011; Schawinski et al. 2011; Kocevski et al. 2012), there are AGN surveys that seems to indicate that interactions do not lead to enhancement of nuclear activity (Li et al. 2008). AGN activity in interacting galaxies is no different from that observed for non-interacting galaxies.

The study of the colours of the host galaxy is also important to characterize its nature. It is well known that the colour–magnitude relation for normal galaxies exhibits two sequences. A *red sequence*, populated by massive, bulge-dominated galaxies with older, passively evolving stellar populations, and a *blue cloud*, populated by blue, star-forming galaxies of small and intermediate masses (e.g. Baldry et al. 2004; Weiner et al. 2005). Past studies indicated that the AGN host galaxy lie in the so-called *green valley* that is the transition region between red sequence and blue cloud (Silverman et al. 2008; Treister et al. 2009) and this result suggested that the AGN feedback can be responsible for regulating the star formation moving galaxies from the blue cloud to the red sequence.

The best way to investigate the signature of induced starburst in active galaxies is through the optical spectra of the host galaxies. However, this can be pursued only for a limited number of sources because it requires very efficient spectroscopic capabilities and observations under excellent conditions. This technique therefore has been used with success only for a limited number of objects at relatively low redshift and with a low-luminosity nuclei (see e.g. Nolan et al. 2001; Miller & Sheinis 2003; Canalizo & Stockton 2013). More recently, using integral field units spectrographs, Liu, Zakamska & Greene (2014) and Husemann et al. (2014) studied samples of luminous unobscured (type 1) quasars providing the morphology, kinematics and the excitation structure of the extended narrow-line region to probe relationships with the BH characteristics and the host galaxy.

An alternative approach to obtain clues of recent star formation in the host of quasars is to measure the colours of the host galaxies from the deblending of the nucleus and host components in multicolour images of quasars. Although this cannot use the more powerful spectroscopic diagnostic to envisage the underlying stellar population, this approach can be adopted for a larger sample of targets provided that the multicolour images be available. This was done in past for 19 quasars at $z < 0.2$ by Jahnke, Kuhlbrodt & Wisotzki (2004) who find mixed results and for a large number of $z < 0.3$ BL Lac host galaxies by Kotilainen & Falomo (2004) and Hyvönen et al. (2007) who find bluer than normal hosts. Quasar hosts that are dominated by a disc component appear to have similar colour to that of inactive galaxies while quasars that have hosts dominated by spheroidal component appear bluer than inactive galaxies.

More recently, Matsuoka et al. (2014a, hereafter M14) and Matsuoka et al. (2015) analysed the stellar properties of galaxies hosting optically luminous, unobscured quasars at $z < 0.6$ using Stripe82 images. They focused on the colours of the host galaxy and found that quasar hosts are very blue and almost absent on the red sequence with a marked different distribution from that of normal (inactive) galaxies.

In this paper, we aim to investigate the colours of a sample of ∼50 low redshift $z < 0.3$ QSO using multicolour images obtained by SDSS in the Stripe82 area. This is a stripe along the Celestial Equator in the Southern Galactic Cap. It is 2.°5 wide and covers $-50^\circ \leq \mathrm{RA} \leq +60^\circ$, so its total area is 275 deg^2. Stripe 82 was imaged by the SDSS multiple times since 2000 only under optimal seeing, sky brightness and photometric conditions. The total number of images reaches ∼100 for the S strip and ∼80 for the N strip. The final frames were obtained by coadding selected fields in the *r* band, with seeing (as derived from 2D Gaussian fit of stars and provided by SDSS pipeline) better than 2 arcsec, sky brightness ≤19.5 mag arcsec^{-2} and less than 0.2 mag of extinction. The QSO sample is extracted from a much larger (∼400 objects) sample of low-redshift quasars in Stripe82 for which we performed a complete study of the host galaxies in the *i* band and their large-scale environments (Falomo et al. 2014; Karhunen et al., in preparation). Using the deep coadded SDSS images of Stripe82, we derive the properties in all five SDSS bands of the host galaxies and we compare with a control sample of (non-AGN), inactive galaxies.

The paper is organized as follows: in Section 2, we present our QSO sample. Section 3 describes the analysis of the data and the main properties of the host galaxies and in Section 4 we discuss our results and we compare our findings with those of M14 and other previous studies. We adopt the concordance cosmology with $H_0 = 70\,\mathrm{km\,s^{-1}\,Mpc^{-1}}$, $\Omega_\mathrm{m} = 0.3$ and $\Omega_\Lambda = 0.7$.

2 THE LOW-*Z* QSO SAMPLE

In previous papers of this series, we investigated the properties of the host galaxies (Falomo et al. 2014, hereafter F14) and of the galaxy environments (Karhunen et al. 2014) of a large (∼400) data set of low-redshift ($z < 0.5$) quasars extracted from the fifth release of the SDSS Quasar Catalog (Schneider et al. 2010), based on the SDSS-DR7 data release (Abazajian et al. 2009) and observed in the region of sky covered by the Stripe82 (Annis et al. 2014). These studies were based on the images in the *i* band and allowed us to go about ∼2 mag deeper with respect to the usual Sloan data and make possible the study of the QSO hosts and their environments.

For this multicolour study, we considered only objects at $z < 0.3$ because beyond this limit the characterization of the QSO host galaxies becomes arduous at bluer filters due to the reduced contrast between the host galaxy and the nuclear emission. We did a number of tests to evaluate the possibility to detect and measure reliably the quasar hosts for a significant fraction of the targets at various redshifts and found that the best compromise that maximize the number of objects resolved in all filters (but not for all objects in the *u* band) is to set a redshift limit to $z \sim 0.3$. In fact, while in the *i* filter the fraction of resolved objects can be as high as 70–80 per cent up to $z \sim 0.5$ (c.f. F14; M14) this fraction falls below 50 per cent for filters *g*, *r* and ∼10 per cent in the *u* band.

From our previous sample of 416 QSO (F14) that were extracted from the QSO catalogue (Schneider et al. 2010) and imaged in the S82 region, we extracted those with $z < 0.3$. This yields 60 QSO; however, four are unresolved also in our previous (F14) analysis and are not considered. One object has been removed from the original list due to the presence of a defect in the image. We visually inspected the spectra of the remaining 55 QSO and found that three objects have emission lines typical of LINERS (Hβ FWHM $<$ 1000 km s^{-1} and log([O III] λ5007/H β) < 0, as derived from SDSS SpecLine table)[1] and were eliminated from the sample. Under these assumptions, we are able to construct a sample of 52 QSO, representing the 87 per cent of all QSO in Stripe82 and with $z < 0.3$, for which we can study the colour of the host galaxy. The mean redshift of this subsample is $\langle z \rangle = 0.25 \pm 0.06$ and the average absolute magnitude of quasar host $\langle M_i \rangle = -22.57 \pm 0.65$. The mean luminosity of our low-z QSO is $M_B = -21.8$ as derived from the g apparent magnitude and transformed to the B band using Jordi, Grebel & Ammon (2006) transformations. As expected the sample is dominated by low-luminosity QSO and merge into the region of objects that can be classified also as Seyfert 1 galaxies [classical division between QSO and Seyfert 1 (Schmidt & Green 1983) is $M_B = -22.2$ in our cosmology].

In our previous work on the environment of low-z QSOs (Karhunen et al. 2014), we defined a control sample of galaxies with similar redshift and host galaxy absolute magnitude distributions. To do this, we selected all the objects classified as galaxies i.e. non-AGN (note that this comparison sample includes both star-forming and passive galaxies) in the Stripe 82 data base for which spectroscopic redshifts were determined and were matched in redshift and galaxy luminosity with the sample of QSO hosts (see F14 for details). In order to build a control sample that match the characteristics of our multicolour subsample of 52 QSO, we select all the galaxies with $z < 0.3$ and that are well matched in terms of absolute magnitude of quasar host and redshift distribution. The control sample of galaxies turned out to have 83 objects with a mean redshift $\langle z \rangle = 0.24 \pm 0.05$ and average absolute magnitude of $\langle M_i \rangle = -22.52 \pm 0.68$, indistinguishable from that of the QSO hosts, see Fig. 1.

For all the objects in this comparison sample of inactive galaxies, we obtained from the Stripe82 catalogues the magnitudes in all the five Sloan bands. All these magnitudes, as for the QSO host galaxies magnitudes were corrected for extinction using the SDSS data (Abazajian et al. 2009) and k-corrected using the package KCORRECT (Blanton & Roweis 2007).

3 IMAGE ANALYSIS

For the 52 QSO, we retrieved the calibrated and combined images in all colours (u, g, r, i, z) from SDSS Stripe 82 data set (Annis et al. 2014). These final combined frames were obtained by coadding selected fields that, in the r band, have a seeing (as derived from 2D Gaussian fit of stars and provided by SDSS pipeline) better than 2 arcsec, sky brightness $\mu = 19.5$ mag arcsec^{-2} and less than 0.2 mag of extinction; for this reason in all the five bands the final frames have the same number of exposures coadded. The images used have an average seeing, as given by 2D Gaussian fit of stars in the frame from SDSS, of 1.49 ± 0.10 arcsec in u, 1.41 ± 0.06 arcsec in g, 1.27 ± 0.06 arcsec in r, 1.2 ± 0.07 arcsec in i and 1.25 ± 0.07 arcsec in z.

[1] objects #56 (SDSSJ214817.43+000419.8), #112 (SDSSJ225757.22+002608.3) and #172 (SDSSJ000834.71+003156.1) in F14

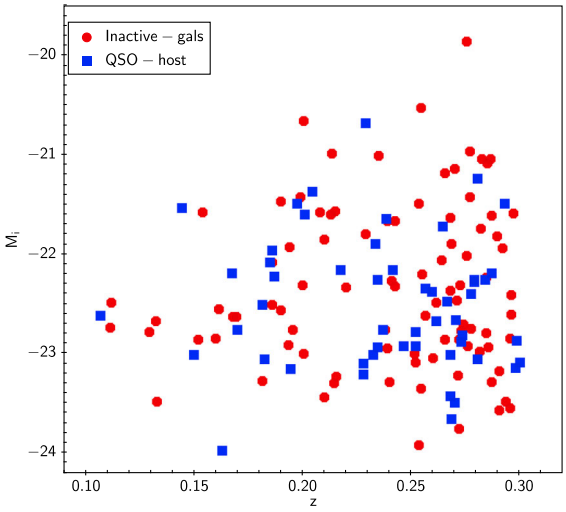

Figure 1. The QSO hosts (blue squares) are compared with inactive galaxies (red circles) in the z–M_i plane (see the text).

In order to derive the properties of the galaxies hosting the QSO, we performed a 2D fit of the images of the QSO following the same procedure adopted for the analysis of the full sample (F14). Briefly, we assume that the image of the QSO is the superposition of two components. The nucleus in the centre and the surrounding nebulosity (the host galaxy). The first is described by the local point spread function (PSF) of the image, while for the second component we assumed a galaxy model described by a Sérsic law convolved with the proper PSF. The analysis of these images was performed using the Astronomical Image Decomposition Analysis package (AIDA; Uslenghi & Falomo 2008).

The most critical aspect of the image decomposition is the determination of a suitable PSF. In the case of SDSS images, the field of view is large enough that there are always many stars in the coadded SDSS image containing the target to properly derive the PSF. As noted in our previous work (F14) the PSF provided by SDSS pipeline, although it is computed from the stars in the frame that are close to the position of the target, it does not account properly for the shape of the PSF at radii larger than about 3 arcsec. The difference between the psField PSF and the true radial profile of stars was shown in fig. 4 of F14. The net effect of using psField PSF is that in all cases where the signal from the quasars extends more than 3 arcsec from the centre of the image the decompositions in terms of point source plus a host galaxy may be systematically biased. In these cases, host galaxies are overestimated and in a number of cases true unresolved sources are confused with resolved objects.

To derive a suitable PSF for the targets in each filter, we selected for each field a number of stars around the QSO and computed a PSF model composed by the combination of three Gaussians and one exponential functions. Then we looked at the fit (χ^2 and visual inspection of the average radial brightness profile) of the model for each PSF stars (c.f. details in F14) in order to remove possible bad stars (poor fit) and fit again all the 'good' stars to produce the final PSF model (see an example, in all filters, in Fig. 2).

Using these PSF models, we then fit all images of the QSO and for all objects we computed the fit of the image of the targets in all filters : u, g, r, i, z (filter 'i' was already available) and then evaluated if the object is resolved (as in the i band) or not in all the remaining filters. We note that, as expected, the nucleus/host ratio increases

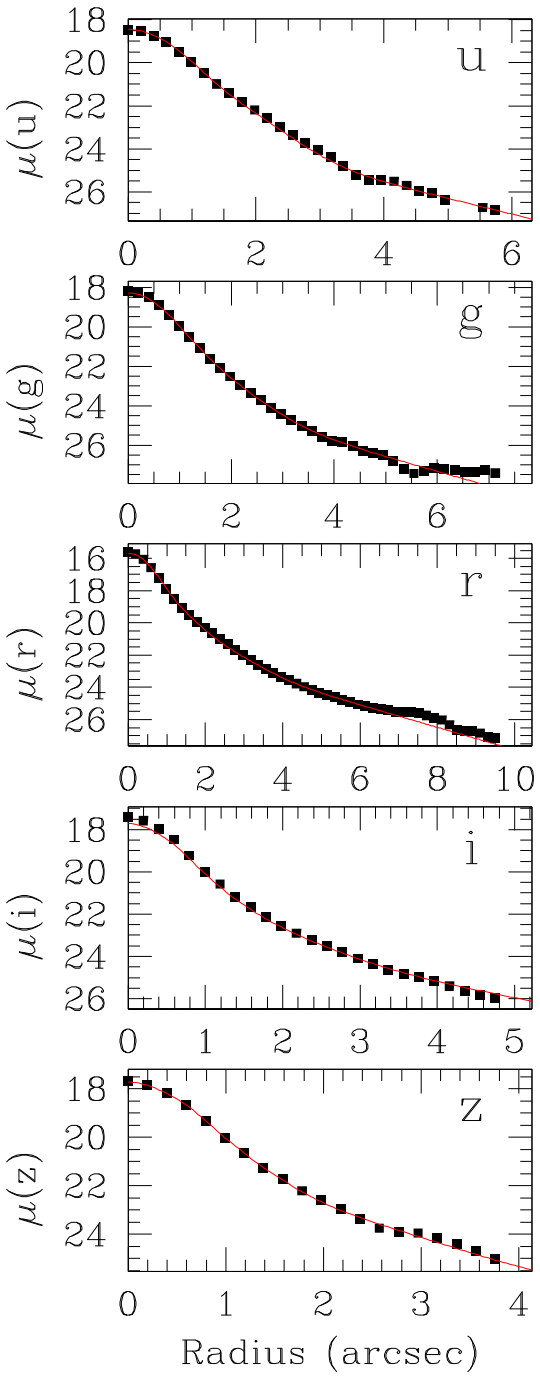

Figure 2. Example (object N.19) of the PSF model (red solid line) compared with the azimuthally averaged radial brightness profiles of some stars in the frame (crosses).

towards the *u* band, leading to more unresolved cases there than in red filters, in fact only ∼50 per cent of objects is found resolved in *u*.

The last step of the analysis is to fit each quasar with a two-component model (point source plus a galaxy). Again we proceeded with the same recipes as in F14. For the coadded images, we assume a readout noise of 9.5 e^- and an average gain of 3.8 e^-/ADU. The term for the statistical noise is given by the coefficient $1/\sqrt{\mathrm{GAIN} \times \mathrm{NEXP}}$ that multiply the root square of the counts. For the residual pattern noise, we assumed 2 per cent value.

The final classification of the targets in each filter was based on the comparison of χ^2 for the two fit (only PSF and PSF + galaxy) and further visual inspection of the fit. From this procedure, we classified all objects as resolved or unresolved. Two QSO are unresolved in all five bands and are present in our list for completeness.

To evaluate the errors on the fit parameters, we performed a number of simulations of the targets and then compared the results of the analysis of the simulate data. For each object, we produced 10 simulated images assuming the best-fitting parameters of the target but with different random noise and including somewhat different levels of the background (based on the uncertainty obtained from the original image). These simulated images were then processed using the same procedure adopted for the original one and the estimate of the error is derived from the comparison of the various best-fitting parameters. From the distribution of the parameter values, we assumed the semi-interquartile range as the error for the derived QSO parameters (see Table 1).

Because our main aim is to study the colours of the host galaxies when we compare colours, we need to derive the *K*-correction for each filter. We estimated the photometric *K*-corrections using the package KCORRECT (Blanton & Roweis 2007), v.4.2, based on the fit of observed photometric points with non-negative linear combination of galaxy spectral templates. We used the default set of five galaxy templates that are based on the stellar population synthesis model of Bruzual & Charlot (2003). *K*-corrections were evaluated at $z = 0$ using the *ugriz* magnitudes corrected for extinction. For half of the sources, the fit was performed using all five bands while for the other half only four filters were used. The quality of the fit is very good($\chi^2 < 1$; see Fig. 3) for 90 and 80 per cent of the galaxies, for the subsamples with five and four bands, respectively.

Similarly for the sample of inactive galaxies we obtain good fit for 85 per cent of the galaxies using in all cases of five bands.

4 RESULTS

In Fig. 3, we show some example of the fit of the Spectral Energy Distribution (SED) of QSO host galaxy using KCORRECT. From these fits, it is also possible to derive some information of the age, stellar content and in particular for the presence of a young component. We also computed the stellar masses from the SED fitting and since KCORRECT assumes a cosmology with $H_0 = 100\,\mathrm{km\,s^{-1}\,Mpc^{-1}}$, the stellar masses were scaled to our cosmology as log (M^*h^{-2}), where $h = H_0/100 = 0.7$. Also for the comparison sample of inactive galaxies, we derived the stellar masses from the SED fitting and in Fig. 4 we show the distribution of masses for both samples with respect to the redshift. The two samples show similar properties in particular, for our sample of resolved objects, we find an average mass of the QSO host galaxy of $\langle \mathcal{M}_* \rangle = 4.28 \pm 2.76 \times 10^{10}\,\mathrm{M}_\odot$ and $\langle \mathcal{M}_* \rangle = 5.27 \pm 3.88 \times 10^{10}\,\mathrm{M}_\odot$ for the comparison sample of normal galaxies. The SED fitting also gives information on the fraction of the total star formation, relative to average star formation rate, that has occurred in the previous 300 Myr (b300) and 1 Gyr (b1000). For QSO hosts and inactive galaxies we obtained both quantities, in Fig. 5 we show the b300 parameter with respect to the stellar mass M^*. As comparison we also plot the distribution of normal galaxies from the SDSS spectroscopic sample at $0.1 < z < 0.3$ derived from the NYU Value-Added Galaxy Catalog[2] (Blanton et al. 2005). The plot indicates very similar properties, in particular

[2] sdss.physics.nyu.edu/vagc/

Table 1. The full sample of resolved objects[1].

Nr	SDSS	z	m_u(host)	m_g(host)	m_r(host)	m_i(host)	m_z(host)
18	205105.02−003302.7	0.3	20.50 ± 0.92	18.83 ± 0.24	18.55 ± 0.12	17.86 ± 0.26	17.85 ± 0.29
19	205212.28−002645.2	0.268	20.14 ± 1.53	18.73 ± 0.18	17.93 ± 0.24	17.65 ± 0.16	17.32 ± 0.27
21	205418.80+004915.9	0.228	–	18.08 ± 0.16	17.63 ± 0.58	17.05 ± 0.61	17.11 ± 0.37
36	211234.88−005926.8	0.235	19.45 ± 0.19	18.36 ± 0.07	17.70 ± 0.14	17.40 ± 0.15	17.14 ± 0.11
40	211832.75+004500.8	0.233	19.50 ± 0.79	18.32 ± 0.18	17.70 ± 0.09	17.30 ± 0.15	17.29 ± 0.17
43	212203.82+001119.2	0.229	–	20.18 ± 0.72	19.56 ± 0.54	19.58 ± 0.57	–
44	212556.26+004539.3	0.281	–	19.54 ± 0.40	19.18 ± 0.21	19.53 ± 0.16	18.95 ± 0.34
51	213110.54−003537.0	0.145	19.61 ± 0.99	18.53 ± 0.10	17.92 ± 0.06	17.63 ± 0.06	17.31 ± 0.21
52	213245.24+000146.4	0.234	–	19.44 ± 0.31	18.72 ± 0.12	18.43 ± 0.12	17.95 ± 0.18
59	215408.71−002744.4	0.218	–	19.05 ± 0.25	18.50 ± 0.37	18.00 ± 0.15	17.79 ± 0.08
61	215516.13+003250.8	0.278	20.77 ± 0.50	19.36 ± 0.24	18.80 ± 0.14	18.34 ± 0.20	18.18 ± 0.37
62	215744.18+005303.6	0.267	20.41 ± 0.72	19.11 ± 0.09	18.47 ± 0.08	18.18 ± 0.08	17.85 ± 0.16
68	215949.01+001004.7	0.271	–	18.82 ± 0.25	18.37 ± 0.38	18.03 ± 0.27	17.73 ± 0.39
89	222315.11−002610.5	0.293	–	20.73 ± 0.43	19.96 ± 0.09	19.39 ± 0.35	19.20 ± 0.59
92	222632.66−005717.7	0.168	19.24 ± 0.66	17.83 ± 0.21	17.37 ± 0.46	17.33 ± 0.39	17.00 ± 0.27
95	222909.81+002527.3	0.228	19.90 ± 1.00	18.21 ± 0.21	17.50 ± 0.09	17.17 ± 0.26	16.81 ± 0.19
113	230007.27+001739.1	0.265	–	–	19.34 ± 0.27	18.91 ± 0.26	18.71 ± 0.29
127	231250.88+001719.0	0.257	–	18.95 ± 0.22	18.41 ± 0.21	18.21 ± 0.25	17.93 ± 0.24
129	231625.39−002225.4	0.298	20.13 ± 0.48	18.42 ± 0.18	18.06 ± 0.10	17.78 ± 0.09	17.51 ± 0.13
130	231711.79−003603.6	0.186	–	18.77 ± 0.25	18.10 ± 0.16	17.80 ± 0.19	17.51 ± 0.11
133	232259.98−005359.2	0.15	18.56 ± 0.20	17.11 ± 0.10	16.45 ± 0.07	16.23 ± 0.07	16.03 ± 0.09
143	233816.42+005029.8	0.183	18.88 ± 0.21	17.66 ± 0.10	16.99 ± 0.07	16.67 ± 0.08	16.35 ± 0.09
154	234932.77−003645.8	0.279	–	18.30 ± 0.14	18.56 ± 0.24	18.50 ± 0.24	18.09 ± 0.39
157	235251.87+003814.9	0.273	–	18.88 ± 0.10	18.16 ± 0.12	17.82 ± 0.09	17.31 ± 0.10
160	235441.54−000448.6	0.279	20.06 ± 0.50	19.41 ± 0.16	18.83 ± 0.18	18.49 ± 0.21	18.84 ± 0.38
161	235457.09+004219.9	0.27	19.66 ± 0.24	18.16 ± 0.14	17.60 ± 0.10	17.18 ± 0.10	16.87 ± 0.21
170	000557.23+002837.7	0.26	–	19.23 ± 0.26	18.46 ± 0.13	18.21 ± 0.28	17.42 ± 0.16
178	001346.52+003402.8	0.274	19.73 ± 0.37	18.55 ± 0.12	18.06 ± 0.10	17.90 ± 0.07	17.66 ± 0.13
189	002752.39+002615.6	0.205	–	19.28 ± 0.27	18.71 ± 0.14	18.63 ± 0.27	18.41 ± 0.32
192	002831.71−000413.3	0.252	19.84 ± 1.05	18.09 ± 0.79	17.77 ± 0.49	17.59 ± 0.64	17.29 ± 0.29
198	003711.00+002127.8	0.235	20.10 ± 0.58	18.45 ± 0.15	18.30 ± 0.07	18.08 ± 0.11	17.74 ± 0.17
199	003723.49+000812.5	0.252	19.57 ± 0.30	18.14 ± 0.09	17.80 ± 0.10	17.72 ± 0.15	17.61 ± 0.12
200	004032.10−001350.8	0.242	–	19.07 ± 0.39	18.38 ± 0.37	18.24 ± 0.32	17.92 ± 0.23
229	011254.91+000313.0	0.239	–	19.47 ± 0.24	18.88 ± 0.09	18.73 ± 0.14	18.42 ± 0.15
277	015521.69−004149.8	0.269	19.36 ± 0.31	17.90 ± 0.73	17.34 ± 0.08	17.02 ± 0.07	16.80 ± 0.09
288	015950.24+002340.8	0.163	17.71 ± 0.37	16.53 ± 0.24	15.86 ± 0.10	15.47 ± 0.21	15.26 ± 0.08
309	021359.79+004226.7	0.182	19.56 ± 0.23	18.15 ± 0.10	17.51 ± 0.12	17.20 ± 0.14	17.01 ± 0.18
325	023922.87−000119.5	0.262	–	18.66 ± 0.09	18.20 ± 0.14	17.93 ± 0.26	17.39 ± 0.38
327	024052.82−004110.9	0.247	–	18.27 ± 0.13	17.76 ± 0.20	17.53 ± 0.13	17.29 ± 0.22
332	024340.98−002601.2	0.268	–	18.23 ± 0.07	17.56 ± 0.09	17.23 ± 0.11	16.95 ± 0.09
333	024508.67+003710.7	0.299	–	19.06 ± 0.18	18.35 ± 0.10	18.07 ± 0.13	17.59 ± 0.39
335	024601.25−005937.2	0.201	–	19.03 ± 0.16	18.57 ± 0.21	18.34 ± 0.21	18.03 ± 0.29
339	025007.02+002525.3	0.198	–	19.39 ± 0.38	18.70 ± 0.40	18.42 ± 0.18	18.12 ± 0.29
342	025334.57+000108.3	0.17	–	17.75 ± 0.16	17.07 ± 0.11	16.79 ± 0.09	16.50 ± 0.11
349	025938.15+004216.3	0.195	19.08 ± 0.41	17.57 ± 0.11	16.93 ± 0.08	16.72 ± 0.07	16.32 ± 0.09
358	030639.57+000343.1	0.107	18.01 ± 0.37	16.79 ± 0.08	16.15 ± 0.08	15.83 ± 0.06	15.48 ± 0.12
360	030731.58+001558.4	0.284	–	19.42 ± 0.19	18.67 ± 0.19	18.55 ± 0.12	18.70 ± 0.35
367	031142.02−005918.9	0.281	19.79 ± 0.36	18.47 ± 0.11	18.03 ± 0.12	17.72 ± 0.09	17.67 ± 0.17
375	032213.89+005513.4	0.185	–	18.25 ± 0.35	17.73 ± 0.30	17.67 ± 0.19	17.69 ± 0.31
390	033156.88+002605.2	0.237	–	18.42 ± 0.11	17.60 ± 0.09	17.60 ± 0.14	17.33 ± 0.10
402	033651.52−001024.7	0.187	–	18.42 ± 0.15	17.81 ± 0.10	17.55 ± 0.21	17.26 ± 0.14
411	034430.03−005842.7	0.287	–	19.32 ± 0.27	19.01 ± 0.16	18.64 ± 0.15	18.50 ± 0.15

[1] All the reported magnitudes have been *k*-corrected.

if we consider that QSO hosts are mainly found at $\log(M/M_\odot) > 10$ there are no differences among the two samples.

In Table 1, we list the final apparent magnitudes of the host galaxies. When the galaxy is unresolved in one colour, no magnitude is reported. In column (1), we give the identification number from the sample of F14, in column (2) the SDSS identification, in column (3) the redshift and in columns (4), (5), (6), (7) and (8) the magnitudes in *u*, *g*, *r*, *i*, *z*, respectively. The apparent magnitudes are also corrected for extinction using the values given by the SDSS data base (Abazajian et al. 2009) and *k*-corrected using the prescriptions given above. In Table 2, we list in column (3) the *i*-band absolute magnitude M_i the colours in columns from (4) to (6), in column (7) the mass $\mathcal{M}_*$ (in $\mathcal{M}_\odot$) derived from the SED fitting and in column (8) the BH mass (in $\mathcal{M}_\odot$) from Shen et al. (2013).

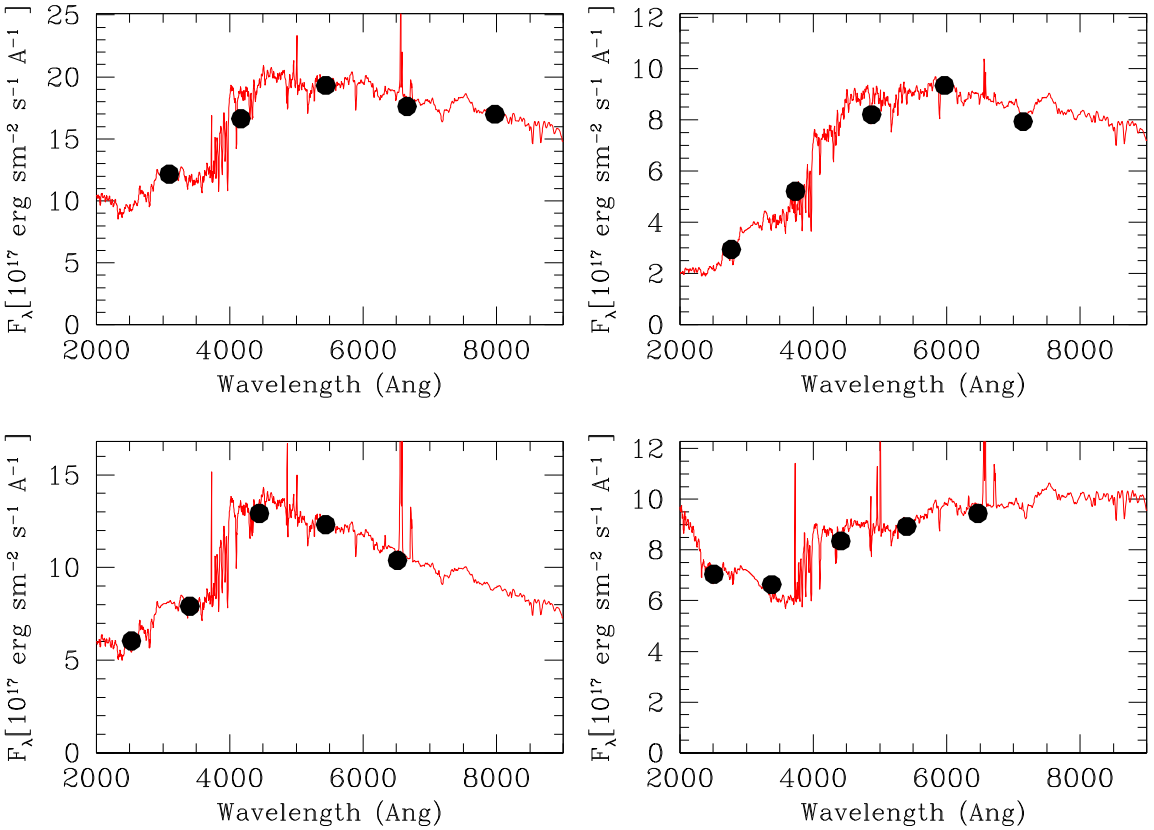

Figure 3. Example of the SED fit (solid line) obtained from the KCORRECT tool for a number of QSO host galaxies with different spectral flux distribution (filled circles).

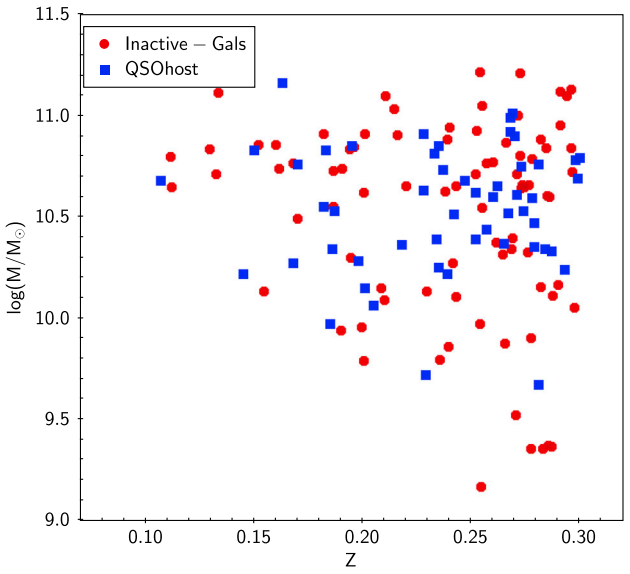

Figure 4. Distribution of the mass of galaxies with respect to the redshift. The mass is estimated from the SED of the galaxies.

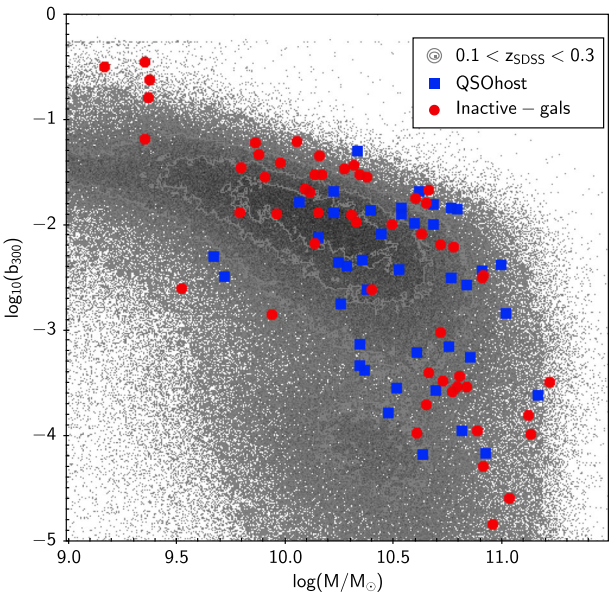

Figure 5. Star formation, relative to average star formation rate, that has occurred in the previous 300 Myr, with respect to the stellar mass (in solar units). Small grey dots and contours are the data for SDSS normal galaxies at $0.1 < z < 0.3$ (Blanton et al. 2005).

4.1 Colours of QSO host galaxies

We were able to resolve all the quasars in the sample in the filters g, r, i and z but one object in g and another in z (see Table 1 for details). For filter u, due to the reduced contrast between starlight and nuclear emission we can resolve the QSO only for 24 objects (46 per cent). In the following analysis, therefore we consider the full sample in all colours but not u and for colour analysis including the u band for a subsample of QSO.

For the whole sample, the average colours are $\langle g - i \rangle$ is 0.82 ± 0.26 and $\langle r - z \rangle$ is 0.55 ± 0.21. For the subsample of

Table 2. The colours of resolved objects.

Nr	z	M_i	$u-g$	$g-i$	$r-i$	$\log(\mathcal{M}_*)$	$\log(M_{\rm BH})$
18	0.3	−23.08	1.66	0.97	0.69	10.79	8.02
19	0.268	−23.01	1.41	1.08	0.29	10.92	8.57
21	0.228	−23.2	–	1.02	0.57	10.63	7.8
36	0.235	−22.93	1.09	0.96	0.3	10.85	8.4
40	0.233	−23.01	1.19	1.01	0.39	10.81	8.46
43	0.229	−20.68	–	0.59	−0.03	9.72	8.16
44	0.281	−21.24	–	0.01	−0.35	9.67	7.67
51	0.145	−21.53	1.08	0.89	0.29	10.22	8.01
52	0.234	−21.89	–	1.01	0.29	10.39	7.95
59	0.218	−22.15	–	1.05	0.5	10.36	8.71
61	0.278	−22.4	1.41	1.02	0.45	10.59	7.79
62	0.267	−22.47	1.3	0.93	0.29	10.52	7.87
68	0.271	−22.66	–	0.8	0.34	10.61	8.47
89	0.293	−21.49	–	1.34	0.57	10.24	7.96
92	0.168	−22.19	1.41	0.51	0.05	10.27	7.86
95	0.228	−23.09	1.7	1.04	0.33	10.91	8.31
113	0.265	−21.72	–	–	0.43	10.37	8.15
127	0.257	−22.34	–	0.73	0.2	10.44	7.85
129	0.298	−23.14	1.72	0.63	0.28	10.78	8.39
130	0.186	−21.96	–	0.98	0.31	10.34	7.81
133	0.15	−23.01	1.45	0.88	0.21	10.83	7.88
143	0.183	−23.05	1.21	0.99	0.32	10.83	8.33
154	0.279	−22.25	–	−0.2	0.05	10.35	8.26
157	0.273	−22.88	–	1.06	0.34	10.75	9.14
160	0.279	−22.27	0.66	0.92	0.34	10.47	8.22
161	0.27	−23.49	1.51	0.98	0.42	10.9	8.8
170	0.26	−22.37	–	1.01	0.25	10.6	8.2
178	0.274	−22.81	1.18	0.65	0.16	10.53	8.47
189	0.205	−21.37	–	0.65	0.09	10.06	7.67
192	0.252	−22.92	1.75	0.5	0.19	10.62	8.71
198	0.235	−22.25	1.65	0.37	0.22	10.25	7.66
199	0.252	−22.78	1.43	0.42	0.08	10.39	7.95
200	0.242	−22.16	–	0.83	0.14	10.51	8.52
229	0.239	−21.64	–	0.74	0.15	10.22	8.31
277	0.269	−23.65	1.47	0.88	0.32	11.01	8.78
288	0.163	−23.97	1.17	1.06	0.39	11.16	8.06
309	0.182	−22.5	1.4	0.95	0.31	10.55	8.93
325	0.262	−22.67	–	0.73	0.27	10.65	8.62
327	0.247	−22.92	–	0.74	0.23	10.68	9.17
332	0.268	−23.42	–	0.99	0.33	10.99	8.84
333	0.299	−22.86	–	1.0	0.28	10.69	8.4
335	0.201	−21.6	–	0.69	0.23	10.15	8.1
339	0.198	−21.49	–	0.97	0.28	10.28	7.96
342	0.17	−22.75	–	0.96	0.28	10.76	8.32
349	0.195	−23.15	1.51	0.84	0.21	10.85	7.41
358	0.107	−22.61	1.22	0.96	0.31	10.68	7.51
360	0.284	−22.25	–	0.86	0.12	10.34	7.69
367	0.281	−23.05	1.31	0.75	0.31	10.76	8.38
375	0.185	−22.08	–	0.57	0.06	9.97	8.04
390	0.237	−22.75	–	0.82	0.0	10.73	8.72
402	0.187	−22.22	–	0.87	0.26	10.53	8.02
411	0.287	−22.19	–	0.68	0.37	10.33	8.0

objects resolved also in u the mean colour $\langle u-g\rangle$ is 1.32 ± 0.25, while the average colours are $\langle g-i\rangle = 0.83 \pm 0.20$ and $\langle r-z\rangle$ is 0.57 ± 0.19 formally indistinguishable from the average values of the full sample (see Table 3).

In Fig. 6, we compare our data, for both QSO hosts and normal galaxies samples with the distribution of normal galaxies from the SDSS spectroscopic sample at $0.1 < z < 0.3$ derived from the

Table 3. The average colours of QSO hosts and inactive galaxies.

Sample	$u-g$	$g-i$	$r-i$	$r-z$
QSO host	1.32 ± 0.25	0.82 ± 0.26	0.26 ± 0.16	0.55 ± 0.21
Galaxies	1.51 ± 0.54	0.88 ± 0.34	0.30 ± 0.12	0.53 ± 0.21

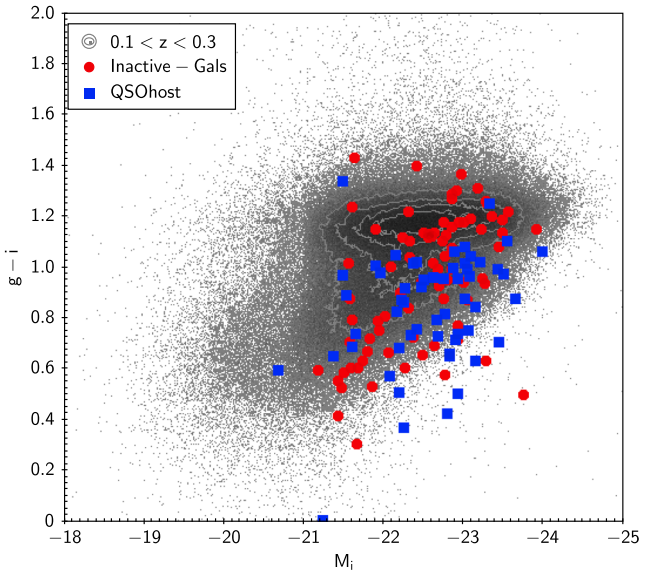

Figure 6. Colour–magnitude plot of the QSO host (blue squares), our sample of normal galaxies (red dots) superimposed to the distribution of the SDSS normal galaxies at $0.1 < z < 0.3$ (small grey dots and contours).

MPA-JHU DR7 catalogue.[3] The two samples span the same range of values; however, if we divide evenly our sample of QSOs it turns out that half of them have $M_i < -22.5$ and the other half $M_i > -22.5$. The average $(g-i)$ colour are 0.82 ± 0.26 and 0.75 ± 0.32, respectively, that compared with similar division for inactive galaxies (also divided at $M_i = -22.5$ produce roughly 50 per cent of subsamples) yields 1.05 ± 0.20 and 0.65 ± 0.32. We also note a clear red sequence of galaxies, mainly populated by inactive galaxies. This contributes to the colour difference, i.e. bluer colour of QSO hosts compared to that of inactive galaxies, at the highest galaxy luminosities. This result for the luminous QSOs is in agreement with the suggestion (see Kauffmann et al. 2003; Jahnke et al. 2009; M14) that the most massive QSO host galaxies (those with $M_i \sim < -22$) are bluer, and thus more star forming, than inactive galaxies of similar luminosity. Both quasar hosts and inactive galaxies of similar mass/luminosity cover a wide range of colours ($0.3 < g-i < 1.3$) that are on average bluer than that of the bulk of normal galaxies.

In Fig. 7, we plot the comparison of the colour–colour diagrams ($g-i$ versus $u-g$) and ($u-g$ versus $r-z$) for quasar hosts and inactive galaxies. The average colours for the sample of inactive galaxies are $\langle g-i\rangle = 0.88 \pm 0.34$, $\langle u-g\rangle = 1.51 \pm 0.54$ and $\langle r-z\rangle = 0.53 \pm 0.21$, formally indistinguishable, within the errors, from those of quasar hosts in our sample. However, we note that the $u-g$ colours of QSO hosts for objects resolved in the u-band span a narrow range in colour and have a smaller scatter of values than the inactive galaxies (see the upper panel of Fig. 7). Finally, we note that the inactive galaxies exhibit a wider colour range in both

[3] http://www.mpa-garching.mpg.de/SDSS/

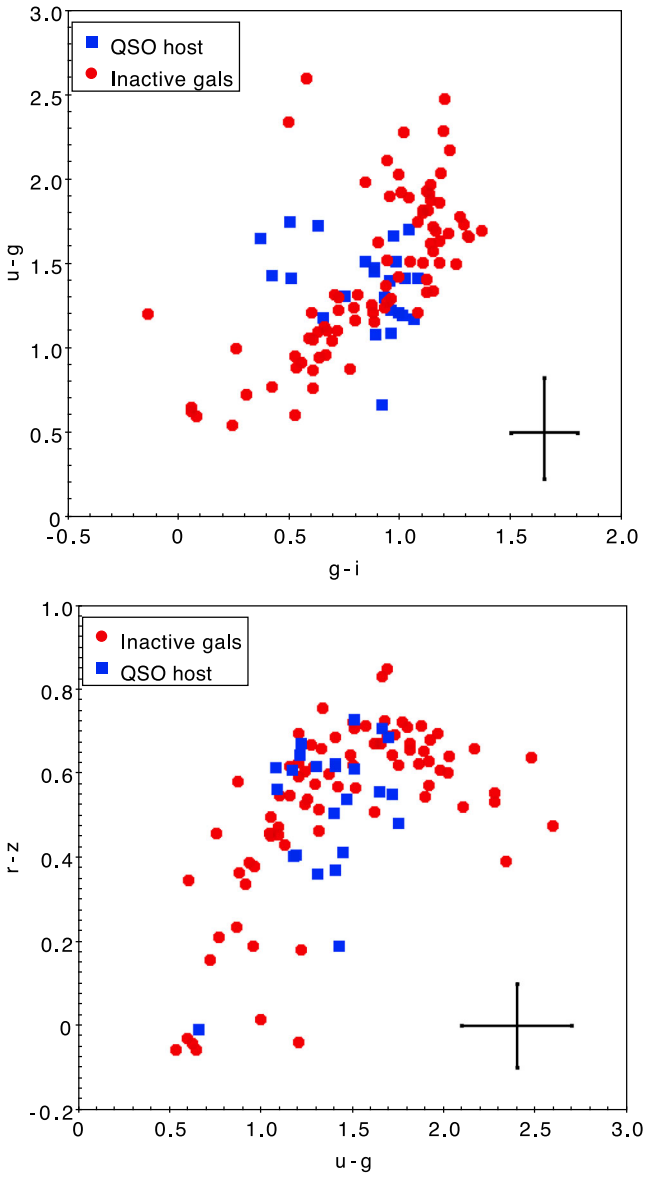

Figure 7. Colour–colour diagrams of the quasar hosts compared to our sample of normal galaxies. In the lower-right corner, the average colour error bars are plotted.

colour diagrams, suggesting that the control sample is a mixture of massive red-sequence galaxies and less massive star-forming blue cloud galaxies.

4.2 Close companion galaxies

For both samples of QSOs and inactive galaxies, we obtained from the Stripe82 catalogues the magnitudes in all bands of the objects classified as galaxies that are at a projected distance from the target less than 50 kpc (at the redshift of the QSO/Galaxy). To minimize the contamination of background objects, we consider as possible companions only the objects with $r < 22.5$ i.e. four magnitudes fainter that the average r-band magnitude of our active or inactive galaxies. In Table 4, we give the statistic of the number of companions found in both samples and in Fig. 8 we show the distribution of the projected distance (derived using the redshift of the targets) versus the r-band apparent magnitude of the close companion for both QSOs and galaxies.

The comparison of the statistics of the close companions for both QSO and matched inactive galaxies sample do not show significative differences (see Fig. 8). There is the 35 per cent of QSO and 39 per cent of galaxies that do not have close companions and the percentages of objects in both samples that have 1 (∼31 and ∼29 per cent) or 2 (∼25 and ∼22 per cent) companions are very similar. Finally, only ∼10 per cent of the remaining objects in both samples have more than three companions (see Table 4). On average the r magnitudes of the companions are very similar ($\langle r \rangle = 20.85 \pm 1.27$ for QSO and $\langle r \rangle = 20.36 \pm 1.32$ for the normal galaxies). There is a suggestion that bright ($r < 20$) companion galaxies are more frequent in QSO (∼50 per cent) than in inactive galaxies (∼25 per cent). While this could be associated with the nuclear activity (past merging and/or interaction), a larger statistical sample is required to reach a firm conclusion. The colour–colour plots for the companions for both QSO hosts and Galaxies are shown in Fig. 9. The colour of close companions of QSO and normal galaxies cover the same region in the explored bands. From our comparison, thus there is no signature of bluer colours for the companions of active galaxies with respect to those of normal galaxies of similar mass.

For both QSO and inactive galaxies samples, we also searched for spectroscopic data of the close companions. Only for six objects with at least one neighbourhood we found the redshift of the companion. In four cases (nos. 61, 92, 95 and 192), the companion is a foreground galaxy while for two objects (nos. 130 and 200), the redshift is identical to that of the QSO. For the inactive galaxies, we found similar results. The redshift of companion was found for five objects and only in one case it coincides with that of the target galaxy. We point out that because of the lack of the redshift of the companions we can only compare statistically the frequency of the companions candidates between the two samples. If the majority of the companions are not associated with QSO/galaxy, a possible difference of physically associated companions might be hidden.

4.3 Comparison with previous studies

In this work, we analysed the colour properties of the host galaxies and their immediate environment for a homogeneous sample of low redshift ($z < 0.3$) QSO and compared their properties with those of a similar sample of inactive galaxies. As detailed in Section 3, we are able to resolve the QSO in g, r, i, and z band for >95 per cent of the objects in the sample and for ∼50 per cent also in the u band. This ensures that we are able to explore the colour properties of the host galaxies of QSO with little incompleteness effects due to the increasing fraction of unresolved sources at higher redshift. Another reason to set a low limit ($z = 0.3$) to the redshift of the sample is that with this limit it is possible to extract a significant sample of normal (inactive) galaxies with similar absolute magnitude of the QSO host galaxies.

The colour distribution of QSO hosts covers a region (see Fig. 6) of bluer colour with respect to the bulk of galaxy population (red sequence). The majority of the objects are in the region between the star-forming and the quiescent galaxies (see also Salim et al. 2007). Similar results were reported by Kauffmann et al. (2003) and Jahnke et al. (2004) for a sample of low-z AGN and also by M14 for their sample of QSO in Stripe82. However, when QSO hosts are compared with a matched sample of inactive galaxies the average colours are found very similar and a bluer colour for the quasar hosts appears for the most luminous host galaxies (see Section 4.1)

Table 4. The statistics of close companions.

Sample	0	1	2	>3
QSO	18 (35 per cent)	16 (31 per cent)	13 (25 per cent)	5 (10 per cent)
Galaxies	36 (39 per cent)	27 (29 per cent)	20 (22 per cent)	9 (10 per cent)

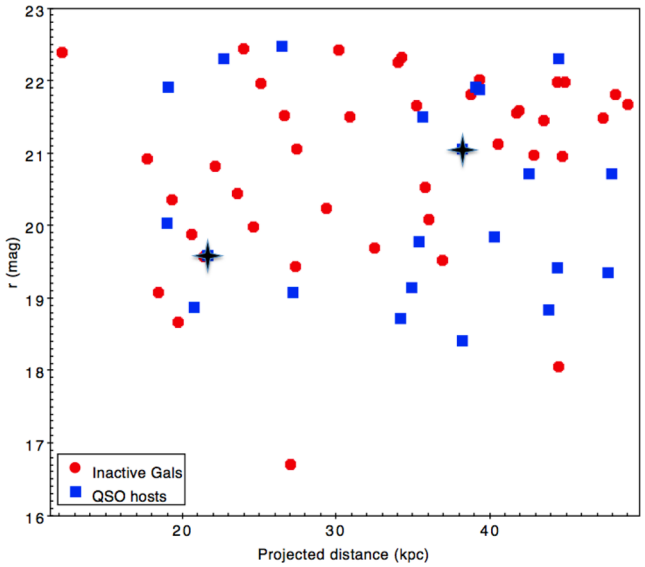

Figure 8. The distribution of distance from the QSO (blue) and inactive galaxies (red) versus the *r* band apparent magnitude of the companion galaxies at projected distance less than 50 kpc. The crosses indicate the two close companions with the same redshift as the QSO.

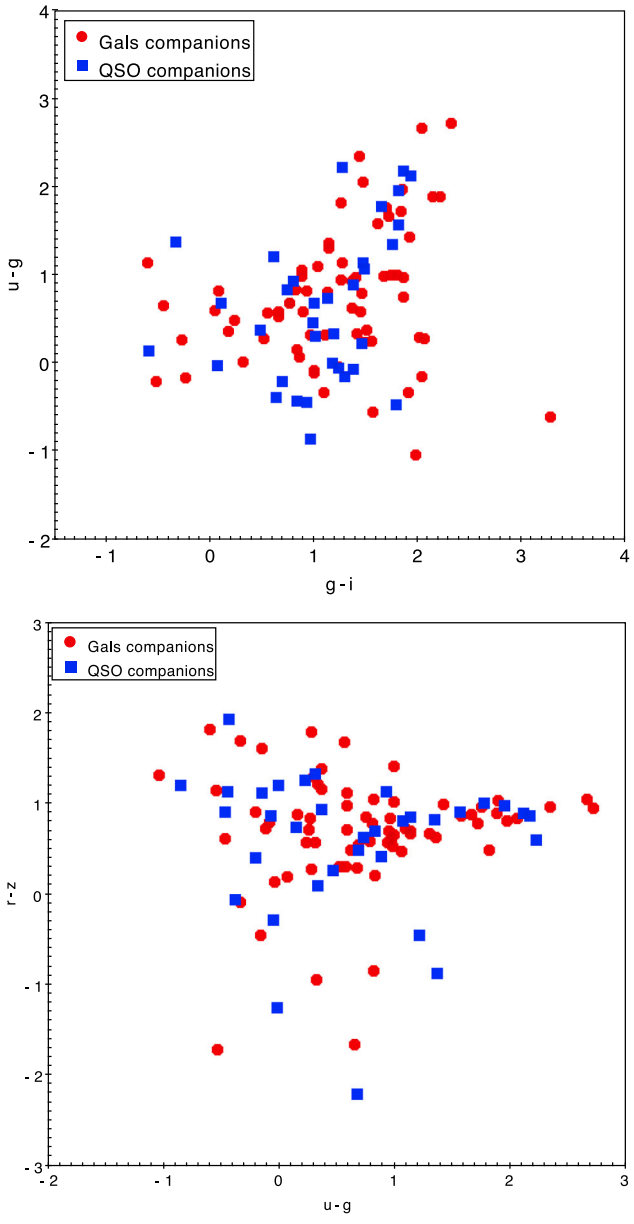

Figure 9. The colour–colour diagrams of the close companions of both QSO and galaxies. Top panel $g - i$ versus $u - g$ and bottom panel $u - g$ versus $r - z$.

The determination of the luminosity of the host galaxies of a sizable sample of quasars allows one to investigate the relationship between the luminosity of the host and the mass of their SMBH. The latter can be derived with the virial method using the width of broad emission lines and the continuum luminosity (see e.g. Shen et al. 2011, 2013). Note that our sample of QSO is limited to $z < 0.3$ where cosmic evolution effects (or selection effects) as those discussed by Schulze & Wisotzki (2014) are negligible (or not detectable). Based on the Stripe82 quasars, M14 find a positive correlation (albeit with a quite large dispersion) between the BH mass and the host galaxy luminosity and/or mass. From their comparison with the local relations derived by Häring & Rix (2004, note that the comparison is with the erratum of M14 i.e. Matsuoka et al. 2014b) for inactive galaxies they conclude that quasar hosts are found to be undermassive for a given SMBH mass. Alternatively, one could interpret this difference as higher mass of the BH for a given mass/luminosity of the galaxy.

This is an opposite result of that found by F14 for a similar sample of S82 QSOs at $z < 0.5$ (see F14; figs 12 and 14). Since the BH mass of QSO is obtained from the same source (Shen et al. 2011), the difference should arise from the evaluation of the luminosity of the host galaxies. The comparison is somewhat complicated by the fact that M14 give absolute magnitudes in AB system and refer to the *i* band assuming objects at $z = 0.3$, while F14 transform the observed magnitudes into rest frame *R* filter (Vega magnitude) in order to be able to compare the host luminosities with previous results secured with *HST* for QSO of similar redshift.

In Fig. 10, we report the relationship between M(BH) and host galaxy absolute magnitude M_i compared with the local relation by Bettoni et al. (2003) that is in good agreement with those by McLure & Dunlop (2002) and Ferrarese (2002) based on similar data sets. The local relation by Bettoni et al. (2003) that is calibrated on the *R* (Vega mag system) filter was transformed into M_i taking into account both the different cosmology assumed and the filter transformations. Contrary to the claim of M14 we do not find a significant positive correlation between the two quantities and find that most of the objects are located below the local relation. This is consistent with our previous finding based on a much larger sample (see F14) and was interpreted as due to a significant disc component

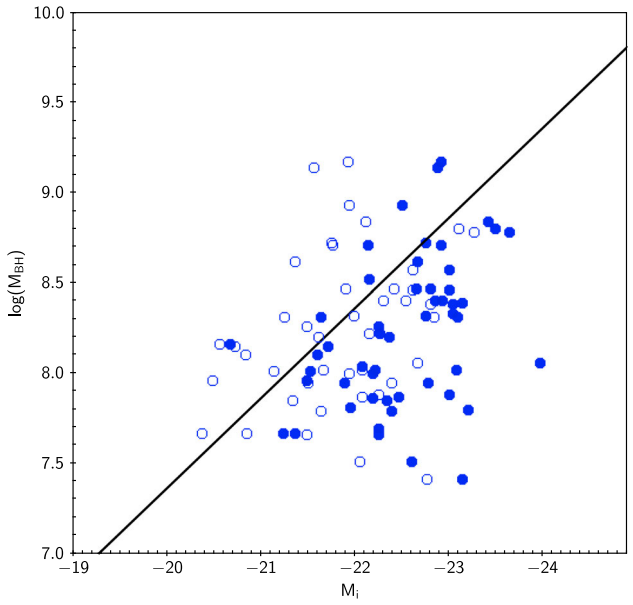

Figure 10. Absolute magnitude (AB) in the *i* band of QSO host galaxies (filled blue circles) versus BH mass (in solar masses) for 52 resolved quasars at $z < 0.3$. The reference (black) solid line is the Bettoni et al. (2003) relation for local (inactive) galaxies for which BH mass was measured. The majority of the host galaxies lie below the local relation and are suggestive of the presence of a significant disc component not correlate with the central BH mass (see the text for details). Open circles refer to the bulge component only.

in the QSO host galaxy (see e.g. Decarli et al. 2012). At low BH masses, a significant disc component has been also recently noted by Sanghvi et al. (2014) and Graham & Scott (2015). For all the objects in the sample, we estimated the bulge to total galaxy luminosity based on morphological classification T of the host galaxy following the scheme in Nair & Abraham (2010). We divided our objects in five morphological classes (see F14 for details) and assigned a bulge/disc ratio ranging from 1 for $T = -5$ to 0.3 for $T = 2$. It turns out that, when the disc component is removed, a more significant relationship is found between BH mass and the bulge component of the host galaxies (see Fig. 10).

5 SUMMARY AND CONCLUSIONS

We have investigated the colour properties of the host galaxies and their close environment from an homogeneous data set of 52 low redshift ($z < 0.3$) quasars using the *u*, *g*, *r*, *i* and *z* SDSS images in the Stripe82 region. The 2D analysis of the images allowed us to well resolve the quasar host for almost all the objects in the sample in the *g*, *r*, *i* and *z* filters and only for half in the *u* band. The colour properties together with the statistics of close companion galaxies of quasars are compared with those of a homogeneous sample of inactive galaxies at similar redshift and comparable luminosity. The following properties of quasar hosts are derived:

(i) The overall mean colours of the QSO host galaxy are indistinguishable from those of inactive galaxies of similar luminosity and redshift. There is a suggestion that the most massive QSO hosts have bluer colours and show a lower star formation rate, in the last 300 Myr, than the control sample of inactive galaxies.

(ii) For about 60 per cent of the quasars, we found companion galaxies at projected distance less than 50 kpc. However, the fraction of objects that have companions at the same redshift of the QSO appears to be only ∼10 per cent. Moreover, the comparison with the companions of inactive galaxies indicates that very similar fractions of companions are present also in non-active galaxies of same luminosity/mass.

(iii) We do not found a significant correlation between the central BH mass and the total luminosity of the quasar hosts. This is contrary to previous claims (M14) based on similar data set that quasar hosts are found to be undermassive for a given SMBH mass. We found that hosts of quasars are more luminous than expected from the local $M_{\rm BH} - M_{\rm bulge}$ relation and interpret it as suggestive of a disc component that is not correlated with the BH mass.

The comparison of colour properties of the quasar host galaxies and of the galaxies in the immediate environments with those of a similar sample of non-active galaxies does not indicate any significant difference. This further supports a scenario where the activation of the nucleus has negligible effects on the global structural and photometrical properties of the hosting galaxies. In particular, the similarity of colours between active and inactive galaxies of similar mass indicates that also the stellar content of these galaxies is virtually unchanged by the presence of an active nucleus.

ACKNOWLEDGEMENTS

We thank the referee for constructive comments that improved this paper. Funding for the SDSS and SDSS-II has been provided by the Alfred P. Sloan Foundation, the Participating Institutions, the National Science Foundation, the US Department of Energy, the National Aeronautics and Space Administration, the Japanese Monbukagakusho, the Max Planck Society and the Higher Education Funding Council for England. The SDSS Web Site is http://www.sdss.org/.

The SDSS is managed by the Astrophysical Research Consortium for the Participating Institutions. The Participating Institutions are the American Museum of Natural History, Astrophysical Institute Potsdam, University of Basel, University of Cambridge, Case Western Reserve University, University of Chicago, Drexel University, Fermilab, the Institute for Advanced Study, the Japan Participation Group, Johns Hopkins University, the Joint Institute for Nuclear Astrophysics, the Kavli Institute for Particle Astrophysics and Cosmology, the Korean Scientist Group, the Chinese Academy of Sciences(LAMOST), Los Alamos National Laboratory, the Max-Planck-Institute for Astronomy (MPIA), the Max-Planck-Institute for Astrophysics (MPA), New Mexico State University, Ohio State University, University of Pittsburgh, University of Portsmouth, Princeton University, the United States Naval Observatory and the University of Washington.

REFERENCES

Abazajian K. N. et al., 2009, ApJ, 182, 543
Annis J. et al., 2014, ApJ, 794, 120
Bahcall J. N., Kirhakos S., Saxe D. H., Schneider D. P., 1997, ApJ, 479, 642
Baldry I. K., Glazebrook K., Brinkmann J., Ivezić Ž, Lupton R. H., Nichol R. C., Szalay A. S., 2004, ApJ, 600, 681
Bettoni D., Falomo R., Fasano G., Govoni F., 2003, A&A, 399, 869
Blanton M. R., Roweis S., 2007, AJ, 133, 734
Blanton M. R. et al., 2005, AJ, 129, 2562
Bruzual G., Charlot S., 2003, MNRAS, 344, 1000
Canalizo G., Stockton A., 2013, ApJ, 772, 132
Cisternas,M.et al., 2011, ApJ, 741, L11
Decarli R., Falomo R., Treves A., Labita M., Kotilainen J. K., Scarpa R., 2010, MNRAS, 402, 2453

Decarli R., Falomo R., Kotilainen J. K., Hyvönen T., Uslenghi M., Treves A., 2012, Adv. Astron, 2012, 782528
Dunlop J. S., McLure R. J., Kukula M. J., Baum S. A., O'Dea C. P., Hughes D. H., 2003, MNRAS, 340, 1095
Falomo R., Treves A., Kotilainen J. K., Scarpa R., Uslenghi M., 2008, ApJ, 673, 694
Falomo R., Bettoni D., Karhunen K., Kotilainen J. K., Uslenghi M., 2014, MNRAS, 440, 476 (F14)
Ferrarese L., 2002, ApJ, 578, 90
Floyd D. J. E., Kukula M. J., Dunlop J. S., McLure R. J., Miller L., Percival W. J., Baum S. A., O'Dea C. P., 2004, MNRAS, 355, 196
Graham A. W., Scott N., 2015, ApJ, 798, 54
Gultekin K. et al., 2009, ApJ, 698, 198
Häring N., Rix H.-W., 2004, ApJ, 604, L89
Heckman T. M., Best P. N., 2014, ARA&A, 52, 589
Husemann B., Jahnke K., Sánchez S. F., Wisotzki L., Nugroho D., Kupko D., Schramm M., 2014, MNRAS, 443, 755
Hyvönen T., Kotilainen J. K., Falomo R., Örndahl E., Pursimo T., 2007, A&A, 476, 723
Jahnke K., Kuhlbrodt B., Wisotzki L., 2004, MNRAS, 352, 399
Jahnke K. et al., 2009, ApJ, 706, L215
Jordi K., Grebel E. K., Ammon K., 2006, A&A, 460, 339
Karhunen K., Kotilainen J. K., Falomo R., Bettoni D., Usleghi M., 2014, MNRAS, 441, 1802
Kauffmann G. et al., 2003, MNRAS, 346, 1055
Kocevski D. D. et al., 2012, ApJ, 744, 148
Kotilainen J. K., Falomo R., 2004, A&A, 424, 107
Kotilainen J. K., Falomo R., Labita M., Treves A., Uslenghi M., 2007, ApJ, 660, 1039
Kotilainen J. K., Falomo R., Decarli R., Treves A., Uslenghi M., Scarpa R., 2009, ApJ, 703, 1663
Kukula M. J., Dunlop J. S., McLure R. J., Miller L., Percival W. J., Baum S. A., O'Dea C. P., 2001, MNRAS, 326, 1533
Li C., Kauffmann G., Heckman T. M., White S. D. M., Jing Y. P., 2008, MNRAS, 385, 1915
Liu G., Zakamska N. L., Greene J. E., 2014, MNRAS, 442, 1303
McLeod K. K., Rieke G. H., 1995, ApJ, 454, L77
McLure R. J., Dunlop J. S., 2002, MNRAS, 331, 795
Matsuoka Y., Strauss M. A., Price T. N., III, DiDonato M. S., 2014a, ApJ, 780, 162 (M14)
Matsuoka Y., Strauss M. A., Price T. N., III, DiDonato M. S., 2014b, ApJ, 789, 91
Matsuoka Y. et al., 2015, AJ, 811, 91
Miller J. S., Sheinis A. I., 2003, ApJ, 588, L9
Nair P. B., Abraham R. G., 2010, ApJ, 714, L260
Nolan L. A., Dunlop J. S., Kukula M. J., Hughes D. H., Boroson T., Jimenez R., 2001, MNRAS, 323, 308
Pagani C., Falomo R., Treves A., 2003, ApJ, 596, 830
Ridgway S., Heckman T., Calzetti D., Lehnert M., 2001, ApJ, 550, 122
Salim S. et al., 2007, ApJS, 173, 267
Sanghvi J., Kotilainen J. K., Falomo R., Decarli R., Karhunen K., Uslenghi M., 2014, MNRAS, 445, 1261
Schawinski K., Treister E., Urry C. M., Cardamone C. N., Simmons B., Yi S. K., 2011, ApJ, 727, L31
Schmidt M., Green R. F., 1983, ApJ, 269, 352
Schneider D. P. et al., 2010, AJ, 139, 2360
Schulze A., Wisotzki L., 2014, MNRAS, 438, 3422
Shen Y. et al., 2011, ApJS, 194, 45
Shen Y. et al., 2013, ApJ, 778, 98
Silverman J. D. et al., 2008, ApJ, 675, 1025
Treister E. et al., 2009, ApJ, 693, 1713
Uslenghi M., Falomo R., 2008, in Di Ges V., Lo Bosco G., Maccarone M. C., eds, Proc. 6th Int. Workshop on Data Analysis in Astronomy, Modelling and Simulation in Science. World Scientific, NJ, p. 303
Weiner B. J. et al., 2005, ApJ, 620, 595

This paper has been typeset from a TEX/LATEX file prepared by the author.